applied sciences

MDPI

Article

Design of Laminated Seal for Triple Offset Butterfly Valve (350 °C) Used in Combined Cycle Power Plants

Hyo Seo Kwak [1], Hansaem Seong [2], Rivaldo Mersis Brilianto [3] and Chul Kim [3,*]

1 Research Institute of Mechanical Technology, Pusan National University, Busan 46241, Korea
2 Department of Mechanical Convergence Technology, Pusan National University, Busan 46241, Korea
3 School of Mechanical Engineering, Pusan National University, Busan 46241, Korea
* Correspondence: chulki@pusan.ac.kr; Tel.: +82-051-510-2489

Received: 26 June 2019; Accepted: 27 July 2019; Published: 31 July 2019

check for updates

Abstract: In combined cycle power plants (CCPPs), the bypass butterfly valve is a key component to facilitate regulation of exhaust gas energy available at the turbine and to not produce too much boost pressure. The conventional damper valve causes leakage, back flow into the turbine, and damage of the blade, and the existing dual-layered seal with polytetrafluoroethylene (PTFE) and metal should be frequently replaced owing to its low durability and deterioration of mechanical properties under a high temperature. This study devised a triple offset butterfly valve with a new type of seal by alternatively laminating stainless steel and graphite to improve valve performance at the high temperature (350 °C). The slope angles of the seal contact surface to prevent friction were calculated using the mathematical models of the triple offset. Thermal-structure coupled analyses by varying the number of graphite and thickness were conducted, and the seven-layer model with the graphite thickness of 0.8 mm, which shows airtightness and smooth operation, was chosen. The contact stresses behaviors of the graphite at 350 °C and at −196 °C were investigated, and it was found that the graphite is in charge of improving driving performance of the disc at the high temperature and sealing performance at the cryogenic temperature. The performance tests and the field tests of the suggested model verified its performance at the working temperature.

Keywords: bypass butterfly valve; laminated seal; graphite; triple offset; airtightness; thermal-structural coupled analysis; contact stress

1. Introduction

As global warming and the depletion of energy resources have intensified, the growth in worldwide energy demand currently faces the difficulty of installing new power generation facilities as a result of limited funding and the strengthening of environmental regulations. Thus, combined cycle power plants (CCPPs), which consist of gas turbines and steam turbines, are becoming more important as the global demand for electrical power increases [1,2]. CCPPs manipulate discarded heat energy and store in hot gas into rotational energy, and the gas turbine compresses air and mixes it with fuel that is heated to a high temperature. The hot air–fuel mixture moves through the gas turbine blades to make them spin, and then the fast-spinning turbine drives the generator that converts a portion of the spinning energy into electricity [3–5]. With the stoichiometric burn, the power output of turbine drops sharply for flow rates above a critical value as a result of aerodynamic losses produced by the rotor blade stalling, and the turbine performs poorly in excessive load and exhaust gas pressure-states, which brings about a decrease in energy production.

In order to prevent the above problems, the bypass system facilitates the regulation of the exhaust gas energy available at the turbine wheel, and thus allows the turbocharger to be controlled and to not produce too much boost pressure. In this system, the bypass valve, which is mounted between the chamber and the atmosphere in parallel with the turbine, limits the maximum pressure in the chamber to prevent the instantaneous air flow rate through the turbine from exceeding the values above which aerodynamic stalling at the rotor blades would produce a severe fall in power output [6–8]. As the modern CCPPs require an increase of exhaust pressure in order to fulfill the restrictions of pollutant emission and to improve energy productivity, the following complementary functions have to be taken into account while designing the bypass valve: resistance to the harsh engine boundary conditions (temperature of 350 °C and working pressure of 1 MPa); smooth operation of the disc during opening and closing; and maintenance of sealing in closed valve operation to maximize gas energy directed to the turbine [9,10].

In the damper valve, which had been used in the existing bypass system, thermal deformations and stress concentrations occurred at a high temperature because there is no offset of the disc rotary axis from the seal. Also, a gap between the body and the disc due to absence of seal caused leakage, back flow into the turbine, and damage of the blade, as illustrated in Figure 1.

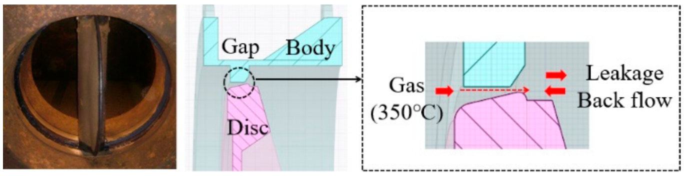

Figure 1. The existing damper valve.

The dual-layered seal with polytetrafluoroethylene (PTFE) and metal had been adopted to solve the above-mentioned problems, but PTFE should be frequently replaced owing to its low durability. Metal has a worse sealing performance than PTFE [11,12], and its mechanical properties are deteriorated at the high temperature [13], so new sealing material, particularly composite material, is needed to improve the sealing ability and durability of other original seals.

The existing single and double offset butterfly valves (SOBV and DOVB) have simple geometric structures to be easily manufactured, but rubbing and friction between the seal and the disc cause life shortening and wear of the seal during opening and closing, as shown in Figure 2. Therefore, this study applies the triple offset (radial eccentricity, axis eccentricity, and cone axis angle eccentricity) butterfly valve (TOBV), whose surface of the seal is in full contact when the valve is fully closed. This eliminates galling and minimizing seal wear and rubbing for long life and tight shut-off.

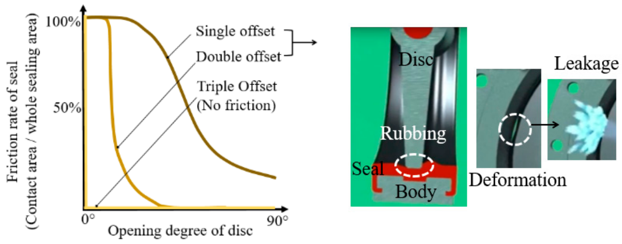

Figure 2. Friction and rubbing occurring at the single and double offset butterfly valves (SOBV and DOVB).

In the previous studies related to the TOBV, Chen determined suitable triple eccentricities to improve the seal performance, and checked the static and dynamic interference through motion simulation [14]. Liang developed a computer programs for calculate the feasible the three eccentricities and the value of the cone's half angle [15]. Kan provided a criterion for non-interference for the metal seal pair considering the radial offset, the diameter of valve disc, the sealing thickness, and the cone angle of the sealing surface [16]. Bodhayan validated the PTFE seal design for gas lift valves through checking leakage amount and performed finite element analysis (FEA) on the seal design under a high pressure to predict the sealing contact pressures [17]. Ping implemented FEA with different sealing ring surface using the numerical method of symmetrical penalty function. The sealing ring surface and the sealing ratio pressure were suggested to enhance the sealing performance of the rotating ball valve with double direction metal sealing [18]. Ahn proposed a design criterion to ensure the seat tightness in which the contact pressure between the metal seal and the valve disc would be compared with the fluid pressure, and mechanical behavior of a flexible solid metal seal for a cryogenic butterfly valve was investigated [19]. However, there were deficiencies of previous works in relation with design of laminated seal in TOBV to possess good sealing property, operability of the disc, and capability of withstanding high temperatures.

In this paper, a study on performance enhancement of the triple-offset butterfly valve used in the bypass system of a CCPP's gas turbine was conducted. After calculating the slope angles of the contact surface to eliminate rubbing on the seal contact surface, with them, the mathematic model of triple-offset was generated. In order to solve the problems of the existing valve, a laminated seal was devised by substituting PTFE for graphite, which is known to excel in extreme conditions, withstanding heat and pressure. The technique for the thermal-structural coupled analysis was established to consider thermal deformation because of exposure to the high temperature (350 °C), and the maximum contact stresses at the contact surface of the seal were derived by varying the number of graphite layers and thicknesses, slope angle of the contact surface (66.1° and 86.1°) calculated and temperature (22 °C and 350 °C). On the basis of the analysis results, the seven-layer model with the graphite thickness of 0.8 mm was suggested to guarantee not only airtightness, but also smooth operation of the disc, and the structural reliability was evaluated. When the contact stresses' behavior of the graphite at 350 °C was compared with that at −196 °C, it was found that the graphite is in charge of improving driving performance of the disc at high temperature and sealing performance at cryogenic temperature. The internal pressure, leakage tests were implemented based on the international regulation, and the actual verification experiment for three months proved the durability and suitability for the actual working environment.

2. Materials and Methods

2.1. Operating Principle and Theoretical Analysis of Triple Offset Butterfly Valve

2.1.1. Structure of Triple Offset Butterfly Valve

The geometry of the triple offset butterfly valve and its component is shown in Figure 3. The disc rotates by the actuator to control amount of the exhaust gas, and the shaft connects the valve body to the actuator. The sealing part consists of the laminated seal and the retainer.

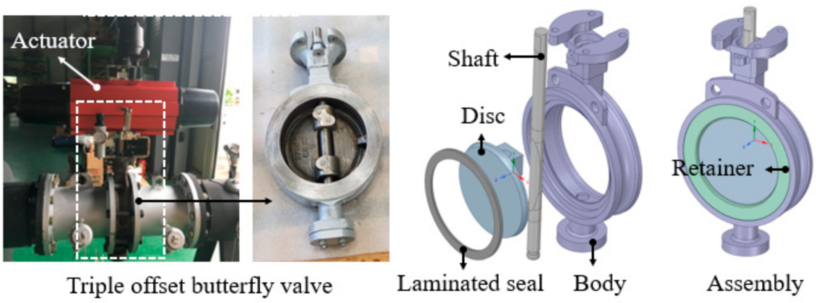

Figure 3. Structural of triple-offset butterfly valve.

2.1.2. Sealing Mechanism of Laminated Seal

This study devised a laminated seal by insertion of graphite with metal (A240–316) to aide in strength and stability for extremely high temperature applications, as shown in Figure 4. To achieve tight shut-off, the disc is driven into the valve body using larger and more expensive actuator than that used with other valve designs, thereby it is necessary to design a shape of laminated seal to achieve the high sealing property and smooth driving with low torque [20].

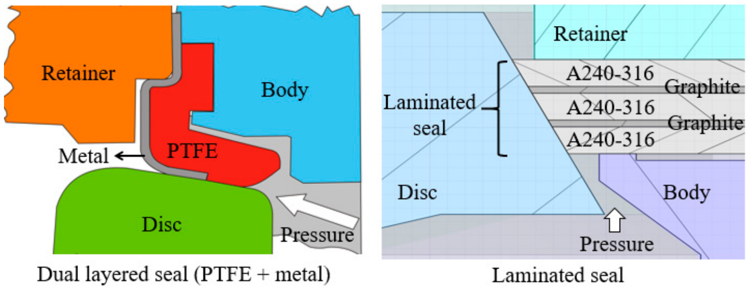

Figure 4. Existing dual seal and new laminated seal. PTFE, polytetrafluoroethylene.

A working pressure of 1 MPa is imposed inside the valve and then produces contact stress on the contact surface between the seal and the body at the final shut-off position. When the working pressure ($P_{working}$) is higher than the contact stress ($P_{contact}$), the fluid is squeezed into the sealing clearance; otherwise, sealing performance is guaranteed as expressed.

2.1.3. Mathematical Modeling of TOBV Seal Pair

Conventional single offset valve with center shaft, which penetrates a seal, is suitable for low temperature and low pressure services only, and double offset valve with eccentric shaft results in an uninterrupted seal that can be used at higher pressures and temperatures, but the friction and seal wear deteriorate sealing performance.

In the triple offset valve, both the seal and the disc are surfaces of a cone that is sectioned at an angle. The valve shaft is located slightly to one side of the seal center and above the plane of the seat, and its rotation center is also offset from the axis of the imaginary cone that extends from the surface of the seat. When the valve is closed, the surfaces of the seal and the disc are in full contact at all points, and opening the valve results in the disc moving away from the seal at all points, eliminating galling and minimizing seal wear due to non-rubbing sealing surfaces for long life and tight shut-off. The three separate offsets are designed in the butterfly valve, as shown in Figure 5.

Offset 1 (H): The shaft is offset from the seal plane providing an uninterrupted sealing surface.

Offset 2 (E): The centerline of disc is offset from the centerline of the shaft allowing the disc to freely lift off and away from the seal during opening.

Offset 3 (γ): The centerline of seal cone with conical angle of 2α is offset by $\gamma°$ from the centerline of the body to eliminate rubbing on the contact surface during opening and closing, thereby rotating the disc without interference [21].

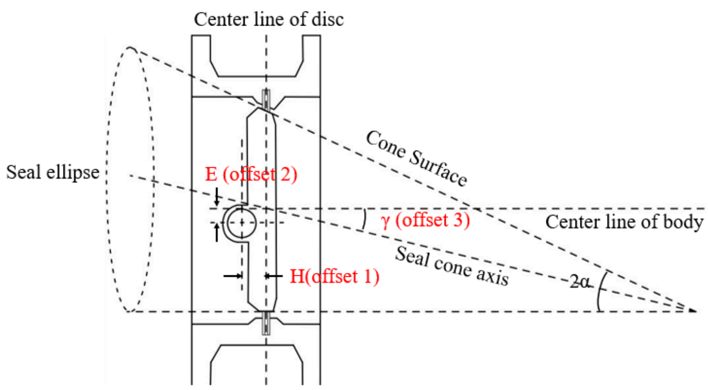

Figure 5. Scheme of the triple-offset butterfly valve.

A coordinate system is established by taking the apex of the cone, and the geometry of the triple offset seal pair is shown in Figure 6.

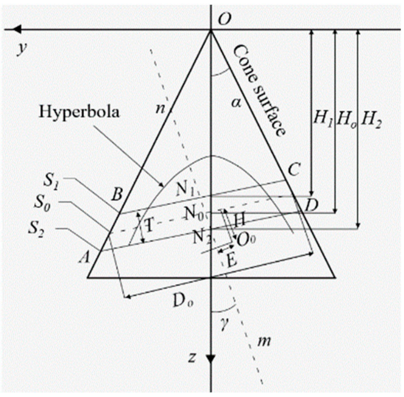

ABCD	:	Seal cone surface
D_0	:	Intermediate diameter of disc
H_0, H_1, *and* H_2	:	Distances from the coordinate origin (*O*) to N_0, N_1 and N_2
N_0, N_1 and N_2	:	Intersections between cone center and S_0, S_1 and S_2
$\overline{mn}$	:	Centerline of valve body
O_0	:	Rotation center of the disc
S_1 , S_2	:	Upper and lower sections of disc
S_0	:	Section of disc center
T	:	Thickness of disc
α	:	Half conical angle

Figure 6. Geometry of triple offset seal pair.

The functions of cone where the disc is situated about *y*-axis are expressed in Equation (1), and the sections of the disc (S_i) in Equation (2) depend on H_i, which are the distances between the coordinate origin (*O*) and N_i, given by Equation (3) (*i* = 1, 2, and 3).

$$y^2 = k^2 \cdot z^2 - x^2, \tag{1}$$

$$z = k_0 \cdot y + H_0 \text{ for } S_0,\ z = k_0 \cdot y + H_1 \text{ for } S_1,\ z = k_0 \cdot y + H_2 \text{ for } S_2, \tag{2}$$

$$H_i = \left(H_0 - \frac{T}{2 \cdot \cos(\gamma)}\right) + \frac{T \cdot i}{\cos(\gamma)}, \tag{3}$$

where k = tan (α) and k_0 = tan (γ). When the sealing surface is truncated by an arbitrary plane that is in parallel with *yOz* plane with its *x*-coordinate as x_0, the equation of the hyperbola (*ajbckd*) shown in Figure 7 is obtained by Equation (4), and the coordinate of two intersection points (x, y_i, z_i) between hyperbola and disc surface (S_i) is obtained by Equation (5).

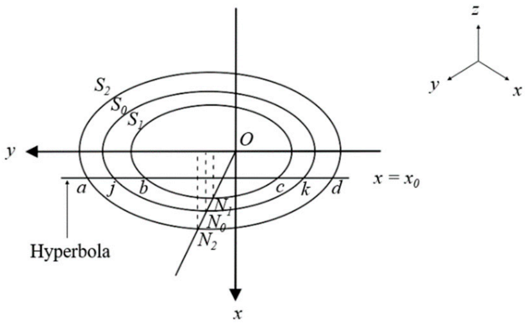

Figure 7. Projection diagram of disc section.

$$\frac{z^2}{\left(\frac{x_0}{k}\right)^2} - \frac{y^2}{{x_0}^2} = 1 \tag{4}$$

$$\begin{cases} x = x_0 \\ y_i = \frac{-k^2 \cdot k_0 \cdot H_i \pm \sqrt{k^2 \cdot k_0^2 \cdot x_0^2 + k^2 \cdot H_i^2 - x_0^2}}{k^2 \cdot k_0^2 - 1} \\ z_i = k_0 \cdot y_i + H_i \end{cases} \tag{5}$$

The elliptical equations for the intersections between the disc cutting planes and the curved surface of cone are expressed by Equation (6).

$$x^2 + y^2 = (k \cdot k_0 \cdot y + H_0)^2,\ x^2 + y^2 = (k \cdot k_0 \cdot y + H_1)^2,\ x^2 + y^2 = (k \cdot k_0 \cdot y + H_2)^2 \tag{6}$$

The intersections between the vertical lines of N_0, N_1, and N_2 with the plane $x = x_0$ are the center point of jk, bc, and ad, and apexes N_i of minor axis of the intersection constitutes the line $\overline{N_iO}$. Friction behavior of TOBV seal pair depends on the following five parameters: offset 1 (E), offset 2 (H), offset 3 (γ), half conical angle (α), and disc thickness (T). During the valve opening and closing, point $P(y, z)$, which is on the hyperbola ab, rotates about O_0 with speed of $\overrightarrow{PN}$ perpendicular to $\overline{O_0P}$, as shown in Figure 8. The angle of θ in Equation (7) is the friction angle between the seal pair ($\overline{PM}$ and $\overline{PN}$), and the angle of β in Equation (8) is between $\overline{PM}$ and the axial line crossing the seal point and parallel with y-axis. The angle of θ_1 in Equation (9) is between $\overline{O_0P}$ and the vertical line crossing the rotary center (O_0). The higher tical line crossing the rotary center (allel with fiv, which means that the disc can rapidly be disengaged from the valve seal, and the friction moment decreases [15].

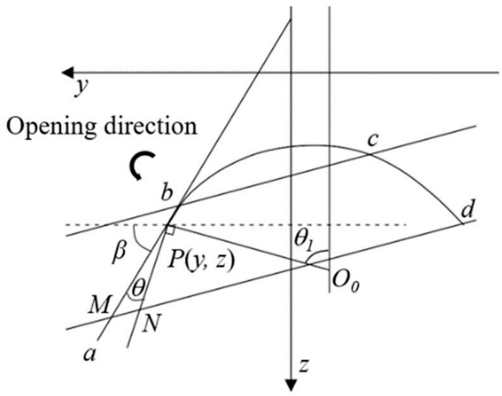

Figure 8. Contact angle of seal pair during closing and opening.

$$\theta = \theta_1 - \beta \tag{7}$$

$$\beta = \arctan\left(\left|\frac{y}{k \cdot \sqrt{x_0^2 + y^2}}\right|\right) \tag{8}$$

$$\theta_1 = \arctan\left(\left|\frac{k \cdot y - k \cdot y_0}{k \cdot z_0 - \sqrt{x_0^2 + y}}\right|\right) \tag{9}$$

2.1.4. Calculation of Slope Angle at Contact Surface

When the TOBV with the inner diameter of 200 mm is subjected to the temperature of 350 °C and the internal pressure of 1 MPa, the diameter and the thickness of the disc, the outer diameter and the thickness of the seal, the three offsets (E, H, and γ), and the half conical angle (α) are given from the international regulations (API609 and ASME B16.10). On the basis of the dimensions shown in Table 1, the geometry of the disc surface was created using commercial software, GEOGEBRA, as follows.

(Step 1) Cone surface is generated by inputting α (13.9°) using Equation (3), as shown in Figure 9a.

(Step 2) When γ (10°), disc thickness (15 mm) is given, H_0 = 369.9 mm, H_1 = 377.5 mm, H_2 = 362.3 mm and rotary center of disc is obtained from Equation (5), and then S_0, S_1, and S_2 are generated using Equation (4), as shown in Figure 9b.

(Step 3) The cone surface is cut by $x = x_0$ (0.05, green plane) to obtain hyperbola in Equation (6), which enables the outer diameter of disc to be 190.1 mm, and then the disc surface is obtained as shown in Figure 9c.

(Step 4) Rotary center of the disc moves by the eccentricity H (23 mm) and E (2.5 mm) to avoid interference between the seal and the disc during opening and closing, as shown in Figure 9d.

(Step 5) The eccentric angle of 10° (γ) of the final triple offset model results in the variation of the slope angle of the contact surface from 66.1° (minimum angle) to 86.1° (maximum angle) in the tangential direction, as shown in Figure 9e.

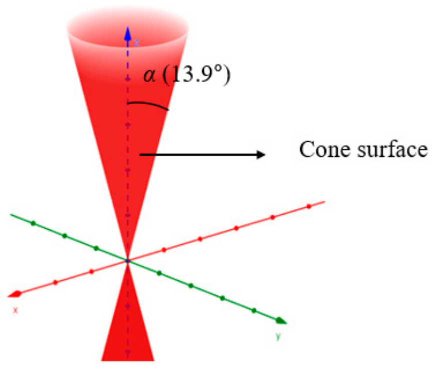

(**a**) Step 1 (Generation of cone surface)

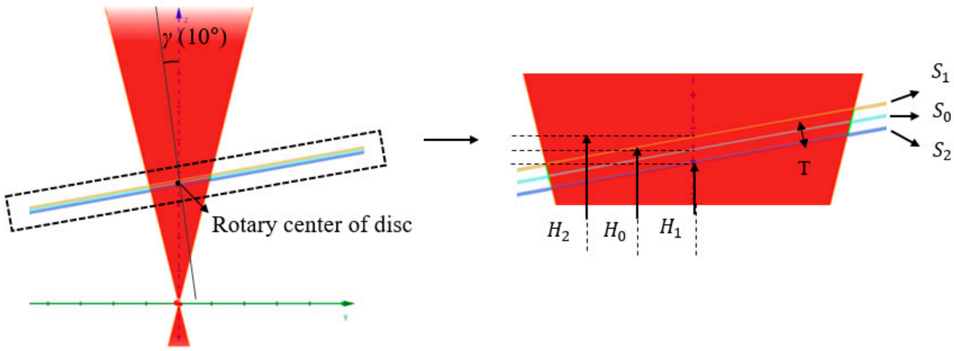

(**b**) Step 2 (Generation of S_0, S_1, and S_2)

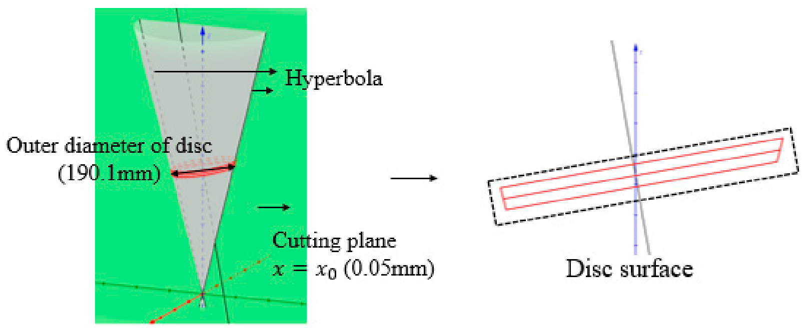

(**c**) Step 3 (fit the outer diameter of disc using hyperbola)

Figure 9. *Cont.*

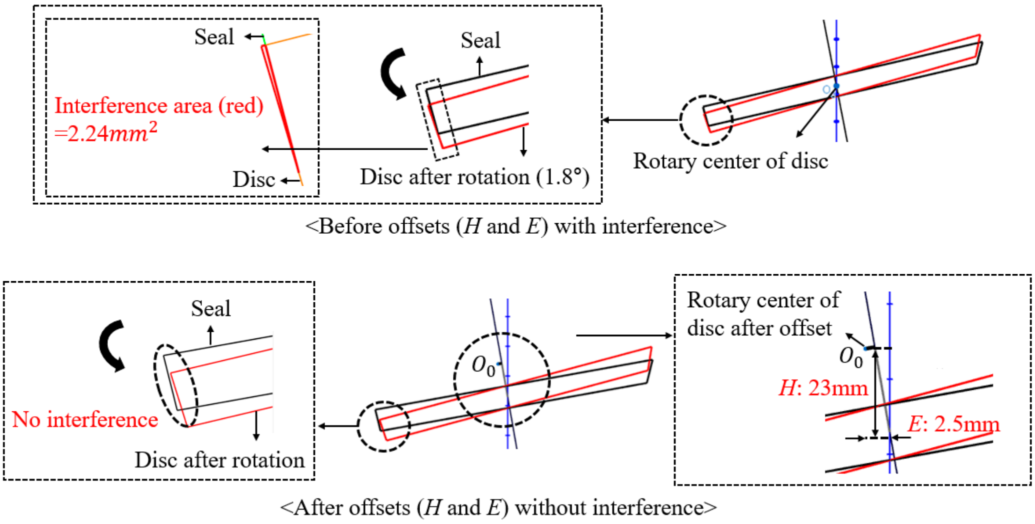

(**d**) Step 4 (move the rotary center of disc by H and E to avoid interference)

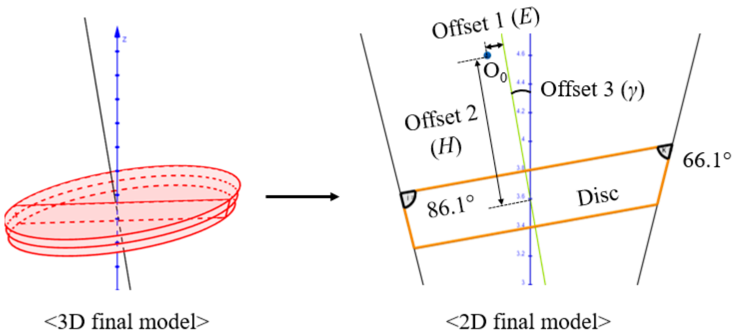

(**e**) Step 5 (final model with variation of slope angle of the contact surface (66.1°~86.1°)

Figure 9. Procedure for generation of slope angle of the contact surface.

Table 1. The value of triple offset butterfly valve (TOBV) parameters.

Diameter of the disc (mm)	190.1	Offset 1, E (mm)	2.5
Thickness of disc, T (mm)	15	Offset 2, H (mm)	23
Outer diameter of the seal (mm)	218	Offset 3, γ (°)	10
Thickness of seal (mm)	7	Half conical angle, α (°)	13.9

2.2. Finite Element Analysis

2.2.1. Geometry and Analysis Conditions

On the basis of the above generated geometry, 2D modeling of the sealing part at final shut-off position was conducted using a commercial software, Inventor 2019, as shown in Figure 10. The contact stress rises with the increase of the slope angle based on the Hertzan theory shown in Equation (10) and Figure 11, so simulations were carried out only in the case of minimum (66.1°) and maximum angle (86.1°).

$$P_{contact} = 0.798\sqrt{\frac{F}{l(\frac{1-v_1^2}{E_1}) + (\frac{1-v_2^2}{E_2})}},\ F = P_{working} \times \cos\varphi \quad (10)$$

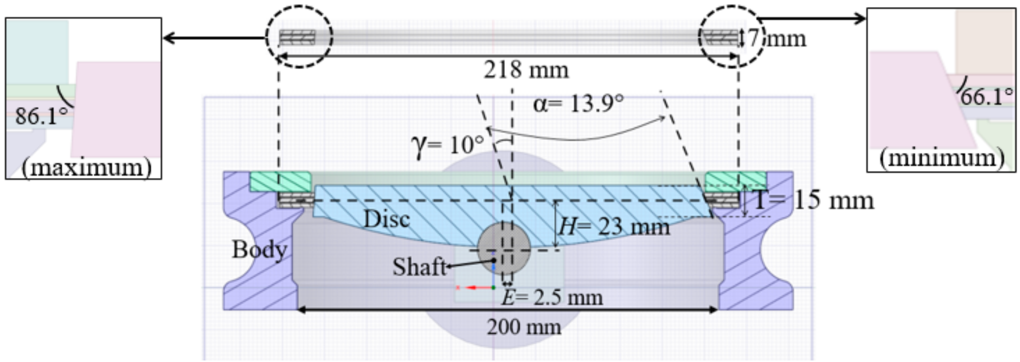

Figure 10. Two-dimensional (2D) geometry of triple offset butterfly valve (TOBV).

F	:	Normal load (N)	v	:	Poison's ratio
l	:	Contact length (mm)	E	:	Young's modulus (MPa)
$P_{working}$	:	Working pressure (MPa)	φ	:	Slope angle of contact surface

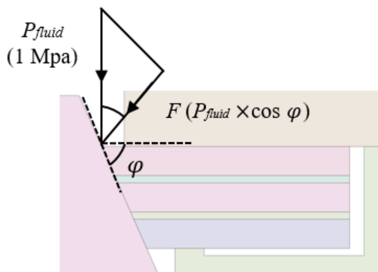

Figure 11. Scheme of normal load (F) acting on the contact surface.

In order to investigate contact stress behavior according to the seal design, a series of finite element (FE) simulations were performed with the different total number of seal layers by laminating alternately the American Society for Testing and Materials (ASTM) A240 Grade 316 stainless steel (SS) and the graphite (G) (1-layer (SS), 3-layer (SS/G/SS), 5-layer (SS/G/SS/G/SS), 7-layer (SS/G/SS/G/SS/G/SS)) and thickness of graphite (0.6 mm~1.2 mm at the interval of 0.2 mm), as shown in Figure 12. Full-thickness (7 mm) of the seal is fixed, so thickness of 1-layer stainless steel depending on that of the graphite was calculated according to the number of laminated layers, as listed in Table 2. The analysis models were simulated according to the temperatures (the room temperature of 22 °C and the high temperature of 350 °C) using commercial finite element software, ANSYS workbench ver. 18.

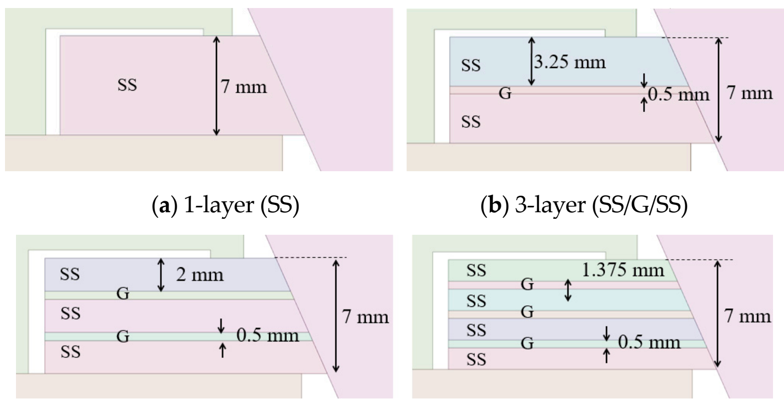

(**a**) 1-layer (SS) (**b**) 3-layer (SS/G/SS)

(**c**) 5-layer (SS/G/SS/G/SS) (**d**) 7-layer (SS/G/SS/G/SS/G/SS)

Figure 12. Analysis model with the different number of layer. SS, stainless steel; G, graphite.

Table 2. Thicknesses of graphite and stainless steel according to the number of layers.

	1-Layer Model	3-Layer Model		5-Layer Model		7-Layer Model	
	Stainless Steel	Graphite	Stainless Steel	Graphite	Stainless Steel	Graphite	Stainless Steel
Thickness (mm)	7	0.6	3.20	0.6	2.13	0.6	1.45
		0.8	3.10	0.8	2.07	0.8	1.39
		1.0	3.00	1.0	2.00	1.0	1.55
		1.2	2.90	1.2	1.93	1.2	1.36

The chemical composition and mechanical properties of the ASTM A240 Grade 316 stainless steel are listed in Table 3. Thermal and mechanical properties of A240–316 (retainer and steel layer), A216 Wrought Carbon with Grade B (WCB) (body), and graphite according to the temperatures (25 °C~350 °C) are listed in Table 4 [16,22,23].

Table 3. Chemical composition of (American Society for Testing and Materials) ASTM A240 Grade 316 Stainless Steel.

Carbon	≤0.08%	Silicon	≤1.0%	Manganese	≤2.0%
Phosphorous	≤0.045%	Sulphur	≤0.030%	Nickel	10~14%
Chromium	16%~18%	Molybdenum	2%~3%	Iron	61.8%~72%

Table 4. Nonlinear material properties according to temperature.

(a) Thermal Conductivity

Temperature (°C)	Thermal Conductivity (W/m·°C)		
	A240–316	A216 WCB	Graphite
25	14.1	11.5	108.4
100	15.4	12.7	106.5
200	16.8	13.8	102.5
250	17.6	14.3	100.3
300	18.3	14.9	98.3
350	19.0	15.4	88.9

(b) Thermal Expansion

Temperature (°C)	Thermal Expansion (10^{-6} m/m·°C)		
	A240–316	A216 WCB	Graphite
25	0	0	0
100	1.3	1.0	0.8
200	3.1	2.3	1.8
250	4.0	3.0	1.8
300	4.9	3.7	1.8
350	5.9	4.5	1.8

(c) Mechanical Property

Temperature (°C)	Elastic Modulus (GPa)			Poisson's Ratio	
	A240–316	A216 WCB	Graphite	A240–316 A216 WCB	Graphite
25	195	202	9.83	0.29	0.21
100	189	198	9.53		
200	183	192	9.53		
250	179	189	9.53		
300	176	185	9.53		
350	172	179	6.619		

Thermal-structural coupled analysis was conducted to calculate contact stress considering deformation caused by the thermal loads and the working pressure (1 MPa). In the thermal analysis, the convective heat transfer coefficient, 3.675×10^{-3} W/mm^2·°C, was employed to the edges of the body, the retainer and the seal, which was exposed to the room temperature, and the thermal load of 350 °C was imposed on the edges, where contact with the working fluid occurred, as shown in Figure 13a. Friction coefficients between the disc and the seal were 0.3 for stainless steel and 0.21 for graphite, respectively, as shown in Figure 13b [19].

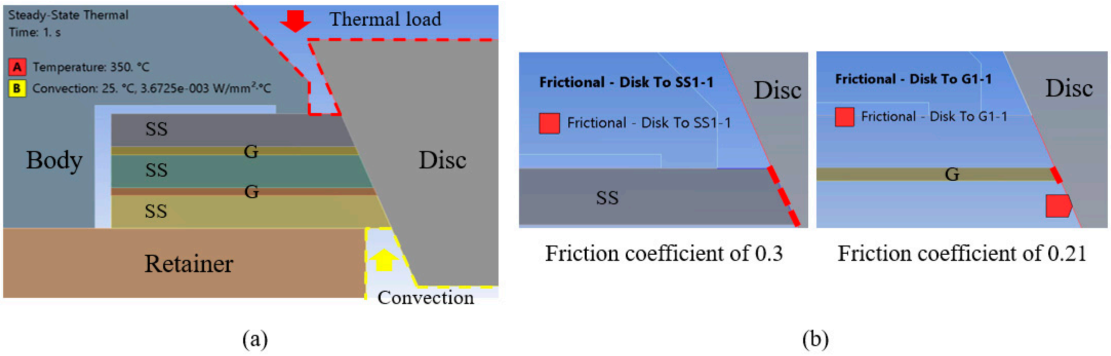

Figure 13. Analysis condition of thermal simulation. (**a**) Temperature and convection, (**b**) friction coefficient. SS, stainless steel; G, graphite.

The global hexagonal grid size of the disc, the body, and the retainer was 1 mm, and that of the seal was 0.5 mm. The denser sizing of 0.1 mm was set up to the edges of the seal and the body at which contact stress occurs as shown in Figure 14a, and the number of nodes was 555,953 and that of elements was 182,554. The orthogonal quality of 98.9% was close to 1, and skewness of 92.8% was close to 0 as shown in Figure 14b, which verifies the FE model.

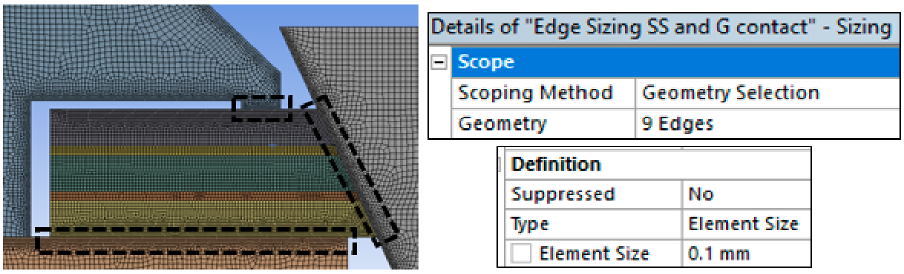

(**a**) Edge sizing

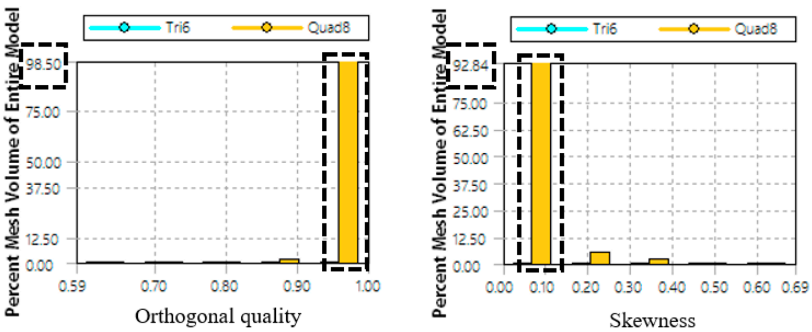

(**b**) Orthogonal quality and skewness

Figure 14. Generation of mesh.

The modeling and outputs of the thermal analysis were coupled to the static structural analysis, as shown in Figure 15a. In this step, deformations at the disc, which were caused by torque applied on the shaft to rotate the disc and to maintain it at the desired position, should be considered [24]. Moment load condition is usable for only axisymmetric geometry in 2D analysis, but is inapplicable because the 2D model is asymmetric because of its eccentricities, thus the maximum deformation in the y-axis (-5.5×10^{-3} mm) at the disc, which was obtained from the 3D simulation, was considered in the 2D simulation, as shown in Figure 15b. Also, the temperature distribution with the maximum value of 350 °C and the minimum of 36.5 °C was imported to the boundary condition, and the working pressure (1 MPa) was applied as shown in Figure 15c. The body and the retainer were fixed, and the x-displacement, which was a relatively very small value (1.7×10^{-4} mm), was not considered.

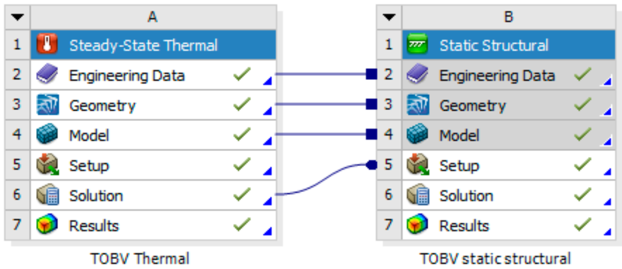

(**a**) Coupling model and result of thermal analysis to static analysis

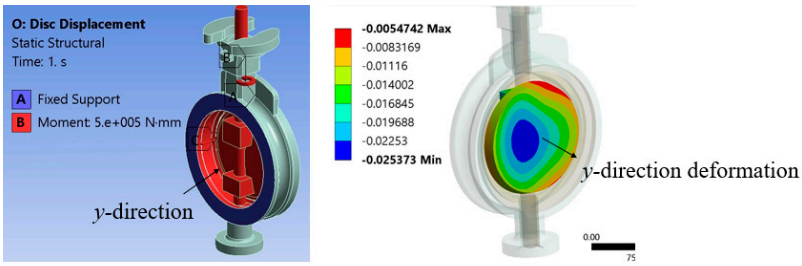

(**b**) Analysis conditions and y-axis deformation distribution caused by torque in 3D simulation

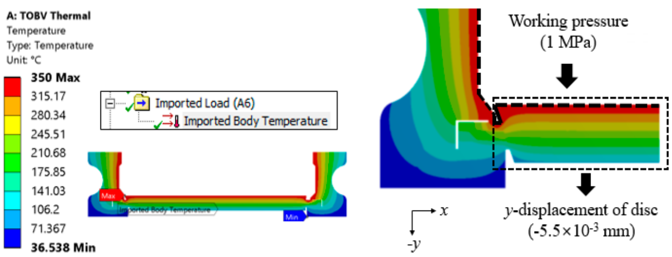

(**c**) Load conditions (temperature, working pressure, and y-displacement)

Figure 15. Analysis conditions of thermal-structural coupled simulation.

2.2.2. Results of the Thermal-Structural Analysis

High contact stress improves sealing performance, while it does not allow the smooth driving of the disc. It is thus necessary to find an effective trade-off between needs for good operation and prevention of leakage. Contact stress, which is a little higher than the working pressure, could guarantee not only airtightness, but also smooth rotation of the disc. Tables 5 and 6 represent the maximum contact stresses for the different seal designs, temperatures (25 °C and 350 °C) and slope angles (66.1° and 86.1°). SS and G indicate stainless steel and graphite, and min and max mean the minimum (66.1°) and maximum (86.1°) slope angles.

Table 5. Maximum contact stresses of stainless steel.

	Graphite	SS_{min} (66.1°)		SS_{max} (86.1°)	
	Thickness (mm)	**22 °C**	**350 °C**	**22 °C**	**350 °C**
1-layer	-	2.00	282.17	0.64	199.71
3-layer	0.6	2.05	169.22	1.16	129.86
	0.8	2.13	154.37	1.16	128.81
	1	2.14	124.61	1.51	115.68
	1.2	2.26	115.37	1.60	95.33
5-layer	0.6	3.40	118.94	1.92	104.14
	0.8	3.62	116.61	2.26	85.61
	1	3.73	113.53	2.66	79.56
	1.2	3.98	104.82	2.67	76.53
7-layer	0.6	3.46	122.55	2.71	68.67
	0.8	3.66	97.15	2.99	66.81
	1	5.09	74.50	4.33	64.33
	1.2	6.33	74.13	4.90	63.02

Table 6. Maximum contact stresses of graphite.

	Graphite	G_{min} (66.1°)		G_{max} (86.1°)	
	Thickness (mm)	**22 °C**	**350 °C**	**22 °C**	**350 °C**
3-layer	0.6	0.26	12.33	0.16	5.03
	0.8	0.28	13.01	0.17	5.67
	1	0.22	8.71	0.16	4.03
	1.2	0.24	7.07	0.15	3.75
5-layer	0.6	0.26	8.12	0.16	3.11
	0.8	0.19	7.20	0.15	2.56
	1	0.22	5.93	0.15	2.14
	1.2	0.21	5.72	0.13	2.10
7-layer	0.6	0.24	7.52	0.18	2.40
	0.8	0.21	4.90	0.18	1.74
	1	0.17	3.60	0.15	0.81
	1.2	0.19	2.73	0.14	0.79

For both stainless steel and graphite, the models with the slope angle of 66.1° showed lower contact stresses than those of 86.1°, which proves that the increases of the contact surface led to a reduction of the peak contact stress, and sealing performance was improved with increasing temperature as a result of thermal expansion.

In respect to the graphite layers, leakages were expected for the all models at 25 °C (G_{min}: 0.19~0.28 MPa, G_{max}: 0.14~0.18 MPa), and there were small changes in contact stress by varying the amount of the graphite, whereas at 350 °C, the larger contact stresses (G_{min}: 12.33~4.73 MPa, G_{max}: 5.03~0.79 MPa) beyond the working pressure were observed. This means that the graphite displayed a sealing effect at high temperature rather than at room temperature, and the contact stress decreases with increment of the number of laminated layer. In respect to the stainless steel layers, the graphite did not withstand the contact force at 25 °C, so the contact stress at the stainless steel increased with more amount of the graphite (SS_{min}: 2.0 MPa → 6.3 MPa, SS_{max}: 1.2 MPa → 4.9 MPa) because the contact force was intensively applied on the stainless steel. On the other hand, at 350 °C, the contact force was distributed to the graphite, so more graphite leads to a reduction of the peak contact stress at the stainless steel (SS_{min}: 169.2 MPa → 74.13 MPa, SS_{max}: 129.9 MPa → 63.0 MPa).

The 1-layer model with the slope angle of 86.1° showed leakage (SS_{max}: 0.61 MPa) at 25 °C, while the excessive contact stresses (SS_{min}: 282.17 MPa, SS_{max}: 199.71 MPa) at 350 °C would disturb smooth operation of the disc. In the 3-layer and 5-layer models, the contact stresses of the stainless steel (SS_{min}: 169.22~115.37 MPa and SS_{max}: 129.86~95.33 MPa for 3-layer, SS_{min}: 118.94~94.82 MPa and SS_{max}: 104.14~76.53 MPa for 5-layer) decreased compared with those of the single layered model

(SS_{min}: 282.17 MPa, SS_{max}: 199.71 MPa) at 350 °C, but they were still too large. The 7-layer model with the graphite thickness of 1.2 mm showed the lowest contact stresses of the stainless steel (SS_{min}: 74.13 MPa, SS_{max}: 63.02 MPa) at 350 °C, but the maximum contact stresses of the graphite were below the working pressure (G_{max}: 0.79 MPa). Therefore, the 7-layer model with the graphite thickness of 0.8 mm was suggested to guarantee not only airtightness, but also smooth rotation of the disc, and its contact stress distributions are shown in Figures 16 and 17.

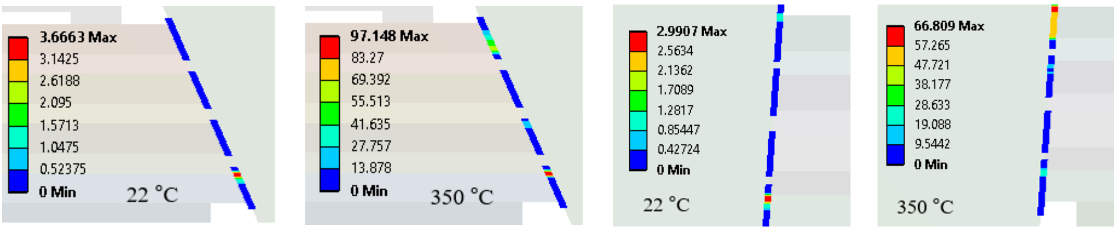

(**a**) Slope angle of 66.1° (**b**) Slope angle of 86.1°

Figure 16. Contact stress distribution at stainless steel of the 7-layer model with graphite thickness of 0.8 mm.

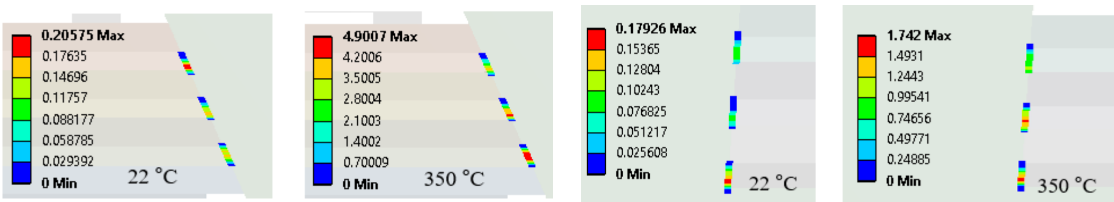

(**a**) Slope angle of 66.1 (**b**) Slope angle of 86.1°

Figure 17. Contact stress distribution at graphite of the 7-layer model with graphite thickness of 0.8 mm.

Analyses results of the new laminated seal at 350 °C were compared to those at the 1-layer, 3-layer, and 5-layer models in Table 7. The maximum contact stresses in case of the slope angle of 66.1° were reduced by 65.5%, 42.6%~15.8%, and 18.3%~7.3%, and those in case of the slope angle of 86.1° were reduced by 66.5%, 48.8%~29.9%, and 35.8%~12.7%, respectively, which means that the shape design of the laminated seal allows to mitigate the excessive contact stress.

Table 7. Comparison of peak contact stress at the new seal with those at the 1-layer, 3-layer, and 5-layer models (350 °C).

Comparison Model	Graphite Thickness (mm)	Reduction of Peak Contact Stress	
		Slope Angle of 66.1°	Slope Angle of 86.1°
1-layer	-	65.6%↓	66.5%↓
3-layer	0.6	42.6%↓	48.6%↓
	0.8	37.1%↓	48.1%↓
	1	22.0%↓	42.2%↓
	1.2	15.8%↓	29.9%↓
5-layer	0.6	18.3%↓	35.8%↓
	0.8	16.7%↓	22.0%↓
	1	14.4%↓	16.0%↓
	1.2	7.3%↓	12.7%↓

2.2.3. Discussions—Effect of Graphite on Sealing Ability

On the basis of the previous study in relation with the cryogenic triple-offset butterfly valve with the laminated seal, which is installed in liquefied natural gas (LNG) marine engine, to control the flow of liquid nitrogen (−196 °C) to liquefy natural gas [25], the contact stress behaviors under the three different temperatures (−196 °C, 25 °C, and 350 °C) were analyzed to discover the graphite effect at each temperature. In the stainless steel layer, the contact stress was increased at 350 °C as a result of undergoing thermal expansion, while in the graphite layer, the larger contact stresses were observed at 350 °C and −196 °C rather than 25 °C, which indicates that the graphite is a favorable for sealing property at severe temperature. As more laminated layers of the graphite, the contact stresses at both graphite and stainless steel decrease at 350 °C, but opposite behavior was observed at −196 °C. It is worth noticing that the graphite contributes improving driving performance of the disc at the high temperature and sealing ability at the cryogenic temperature, as shown in Table 8.

Table 8. Comparison of contact stress behavior of laminated seal at 350 °C with that at −w96 °C.

Temperature (°C)	Change of Contact Stress as More Layers of Graphite		Purpose of Graphite
	Stainless Steel	Graphite	
350	↓	↓	For improving driving performance
−196	↑	↑	For improving sealing performance

2.2.4. Verification of Structural Safety of the Proposed TOBV

In order to verify the reliability of the TOBV with the proposed laminated seal, the 3D thermal-structural coupled analysis was conducted as shown in Figure 18. The simulation conditions (convective heat transfer coefficient, thermal load, friction coefficients, and torque) were the same as in the 2D analysis. Table 9 compares the maximum equivalent stress at each part with the allowable strength [26], and it is expected that all components are not yielded at 350 °C. Also, the contact surfaces of the final model showed the sticking status as shown in Figure 19, so deboning of the seal layers due to the different expansion coefficients does not occur.

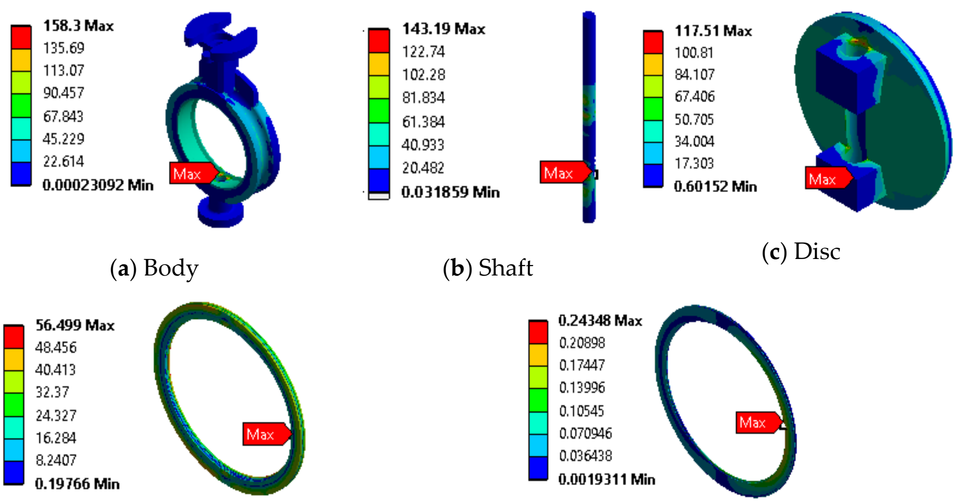

(**a**) Body (**b**) Shaft (**c**) Disc

(**d**) Laminated seal—stainless steel (**e**) Laminated seal—graphite

Figure 18. Equivalent stress distribution in each part of proposed model.

Figure 19. Contact status between stainless and graphite layers.

Table 9. Structural safety of the proposed TOBV.

Part	Allowable Strength (MPa)	Maximum Equivalent Stress (MPa)	Yielding
Body	184.25	158.30	No
Shaft	385.25	143.19	No
Disc	137.35	117.51	No
SS	137.35	56.50	No
G	4.69	0.24	No

3. Prototype and Performance Test

3.1. Internal Pressure and Leakage Tests

The performance tests of the proposed TOBV were conducted using the experimental equipment, based on the regulation of KS B 2304:2001 (General rules for inspection of valves). The boiler and the temperature sensor controlled the temperature of 350 °C, and the pressure gauge checked the internal pressure. In the internal pressure test, the valve body was filled with the water at the half-shut position, and then the internal pressure of 1.7 MPa, which exceeded the working pressure (1 MPa) × 1.5, was maintained for 182 s. In the leakage test, the valve body was filled with the water at the fully shut-off position, and the internal pressure of 1.15 MPa, which exceeded the working pressure (1 MPa) × 1.1, was maintained for 125 s. The results of the flowrate measurement exhibit that there were no leakage and exudation in both tests, as shown in Table 10 and Figure 20.

Table 10. Results of performance tests.

		Internal Pressure (MPa)	Duration Time (s)	Result
Internal pressure test	Regulation	1.5	160	No leakage
	Actual	1.7	182	
Leakage test	Regulation	1.1	125	No leakage
	Actual	1.15	30	

(**a**) Internal pressure and duration time (left: pressure test, right: leakage test)

(**b**) Visual inspection and leakage measurement

Figure 20. Conditions and results of the performance tests.

3.2. Field Test of Proposed TOBV in CCPPs

The prototype of the proposed TOBV was installed at the gas turbine in the CCPPs and was operated for three months to evaluate durability and suitability for the actual working environment. Leakage could not be measured at the rear end of the turbine, so sealing performance of the new model was predicted by comparing its temperature with that of the conventional valve, as shown in Figure 21. Perfect sealing blocks the hot gas flow into the outlet pipe, which allows the temperature in the rear end to decrease. The measurement results show that the gas (350 °C), which entered into the inlet pipe during the disc opening, elevated sharply the temperature at the rear end from 27 °C to 100 °C. After then, the temperature decreased at fully shut-off position, and it kept in an almost steady state. The time to be required for opening and closing the disc was 4.25 s, and its cycle was one day. Temperature of the new model (32 °C) decreased by 20%, compared with that of the conventional one (40 °C), which demonstrates that the proposed laminated seal improved the sealing ability of the TOBV.

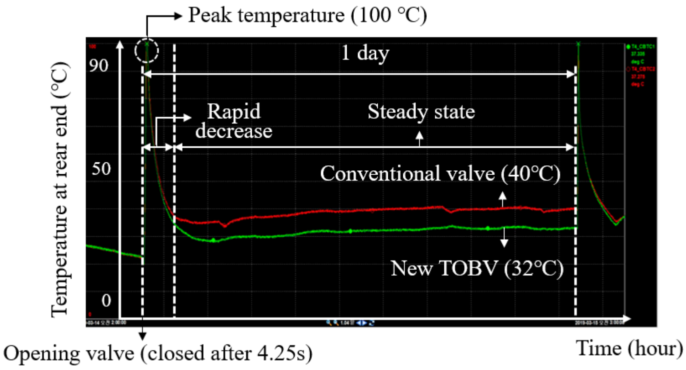

Figure 21. Temperatures at rear end of the new TOBV and the conventional one.

4. Conclusions

This study developed the laminated seal to enhance sealing performance and operability of the TOBV. Our conclusions are summarized as follows.

(1) When the TOBV has the inner diameter of the pipe: 200 mm, the diameter of disc: 190.1 mm, the outer diameter of seal: 218 mm, and the thickness of disc: 15 mm, the three eccentricities (offset 1: 2.5 mm, offset 2: 23 mm, offset 3: 10°) were specified based on the international regulation, and the slope angles of contact surface (66.1° (minimum angle)~86.1° (maximum angle)) for eliminating rubbing were calculated.

(2) Thermal-structural coupled analyses were conducted for the different seal designs (the number of seal layers and graphite thicknesses), temperatures (25 °C and 350 °C), and slope angles (66.1° and 86.1°), and the maximum contact stresses' behaviors at the contact surfaces were investigated as follows:

- It was observed that the increases of contact surface led to a reduction of the peak contact stress, so that sealing performance was improved with increasing temperature as a result of thermal expansion.
- In respect to the graphite layers, leakages were expected for the all models at 25 °C (G_{min}: 0.19~0.28 MPa, G_{max}: 0.14~0.18 MPa), and there were small changes in contact stress by varying the amount of the graphite, whereas at 350 °C, the larger contact stresses (G_{min}: 12.33~4.73 MPa, G_{max}: 5.03~0.79 MPa) beyond the working pressure were observed, which means that the graphite showed a sealing ability at the high temperature rather than at the room temperature.
- In respect to the stainless steel layers, the graphite did not withstand the contact force at 25 °C, so it was intensively applied on the stainless steel whose surface was decreased as the amount of the graphite was increased, and then the contact stresses at the stainless steel were increased (SSmin: 2.0 MPa → 6.3 MPa, SSmax: 1.2 MPa → 4.9 MPa). While at 350 °C, the contact force was distributed to the graphite, and the peak contact stress at

the stainless steel was reduced (SSmin: 169.2 MPa → 74.13 MPa, SSmax: 129.9 MPa → 63.0 MPa) as the amount of graphite was increased.

- The 7-layer model (graphite thickness: 0.8 mm, stainless thickness: 1.15, total thickness of seal: 7 mm, the slope angles of contact surface: 66.1° and 86.1°) was suggested to guarantee not only airtightness, but also smooth rotation of the disc.

(3) More laminated layers of the graphite decreased the contact stresses in both graphite and stainless steel at 350 °C, but opposite behavior was observed at −196 °C, which means the graphite is in charge of improving driving performance of the disc at the high temperature and sealing ability at the cryogenic temperature.

(4) In the field test, which was implemented for three months in CCPPs, the temperature (32 °C) in the rear end of the new model decreased by 20%, compared with that of the conventional one (40 °C), which demonstrates that the proposed laminated seal improved the sealing ability of the TOBV, and its durability and suitability for the actual working environment were verified.

The TOBV with the new laminated seal could improve turbine performance in the high temperature and production of electricity; furthermore, it could be widely applied to various industry fields under the server environments.

Author Contributions: H.S.K., H.S.S., and R.M.B. conceived design method/FEA, analyzed the data, and performed the experiments; R.M.B. performed design and FEA; H.S.K. wrote the manuscript; H.S.S. assisted with FEA; C.K. was in charge of the whole trial. All authors read and approved the final manuscript.

Funding: This research was funded by the research development business funded by the KOREA SOUTHERN POWER CO., LTD (KOSPO)—2017-02. The authors gratefully acknowledge this support.

Acknowledgments: The authors would like to express gratitude to KOREA SOUTHERN POWER CO., LTD (KOSPO for funding and for critical discussion and technical assistance.

Conflicts of Interest: The authors declare no conflict of interest.

Abbreviations

CCPP	Combined Cycle Power Plants
SOBV	Single Offset Butterfly Valve
DOBV	Double Offset Butterfly Valve
TOBV	Triple Offset Butterfly Valve
PTFE	Polytetrafluoroethylene
ASME	The American Society of Mechanical Engineers
API	American Petroleum Institute

References

1. Choi, M.G.; Ryu, J.Y. Numerical Study of the Axial Gap and Hot Streak Effects on Thermal and Flow Characteristics in Two-Stage High Pressure Gas Turbine. *Energies* **2018**, *11*, 2654. [CrossRef]
2. Almutairi, A.S.; Pilidis, P.; Al-Mutawa, N. Energetic and Exergetic Analysis of Combined Cycle Power Plant: Part-1 Operation and Performance. *Energies* **2015**, *8*, 14118–14135. [CrossRef]
3. Rao, A.D. *Combined Cycle Systems for Near-Zero Emission Power Generation*; Woodhead Publishing: Cambridge, UK, 2012; pp. 1–43.
4. Shiraishi, K.; Ono, Y.; Yamashita, Y.; Sakamoto, M. Energy Savings through Electric-assist Turbocharger for Marine Diesel Engines. *Mitsubishi Heavy Ind. Tech. Rev.* **2015**, *52*, 36–41.
5. Najjar, Y.S.H.; Ismail, M.S. Optimum Pressure Ratios for Different Gas Turbine Cycles. *High Temp. Technol.* **1990**, *8*, 283–289. [CrossRef]
6. Brito-Melo, A.; Gato, L.M.C.; Sarmento, A.J.N.A. Analysis of Wells turbine design parameters by numerical simulation of the OWC performance. *Ocean Eng.* **2002**, *29*, 1463–1477. [CrossRef]
7. Falcao, A.D.O.; Vieira, L.C.; Justino, P.A.P.; André, J.M.C.S. By-pass air-valve control of an OWC wave power plant. *J. Offshore Mech. Arct. Eng.* **2003**, *125*, 205–210. [CrossRef]

8. Zanger, J.; Widenhorn, A.; Aigner, M. Experimental Investigations of Pressure Losses on the Performance of a Micro Gas Turbine System, ASME. *J. Eng. Gas Turbines Power* **2011**, *133*, 082302. [CrossRef]
9. Amano, R.S.; Draxler, G.R. High-pressure steam flow in turbine bypass valve system Part 1: Valve flow. *J. Propuls. Power* **2002**, *18*, 555–560. [CrossRef]
10. Khan, M.N.; Tlili, I. Performance Enhancement of a Combined Cycle Using Heat Exchanger Bypass Control: A Thermodynamic Investigation. *J. Clean. Prod.* **2018**, *192*, 443–452. [CrossRef]
11. Stankus, S.V.; Yatsuk, O.S.; Zhmurikov, E.I.; Tecchio, L. Thermal expansion of artificial graphites in the temperature range 293–1650 K. *Thermophys. Aeromech.* **2012**, *19*, 463–468. [CrossRef]
12. Manhani, G.B.; Pardini, C.L.; Neto, F.L. Assessment of tensile strength of graphites by the Iosipescu coupon test. *Mater. Res. Ibero Am. J. Mater.* **2007**, *10*, 233–239.
13. Zhao, C.Y.; Wu, Z.G. Heat transfer enhancement of high temperature thermal energy storage using metal foams and expanded graphite. *Sol. Energy Mater. Sol. Cells* **2011**, *95*, 636–643. [CrossRef]
14. Chen, B.; Fan, Y.G. 3D modeling and Open-close Motion Simulation of the Triple Eccentric Butterfly Valve. *Adv. Mater. Res.* **2011**, *215*, 191–194. [CrossRef]
15. Liang, R.; Jiang, F.; Zhou, X.H.; Yu, S.R.; Du, Z.N. Three-dimension Analysis of the Three-eccentricity Butterfly Valve Metal Seal Pair Interference. *Fluid Mach.* **2003**, *8*, 5.
16. Kan, B.; Ding, J. Criterion for non-interference of solid metal seal pair in double-offset butterfly valve. *J. Braz. Soc. Mech. Sci. Eng.* **2016**, *38*, 1745–1752. [CrossRef]
17. Dev, B.; Samudrala, O.; Wang, J. Characterization of leak rates in thermoplastic barrier valve seals under high static and cyclic pressure loads. *J. Pet. Sci. Eng.* **2016**, *145*, 279–289. [CrossRef]
18. Lei, J.P.; E, J.Q.; Chen, J.M.; Zhang, Y.; Zeng, E.Q.; Chen, H.Z.; Liu, H.; Guo, L.; Su, J.X. Finite element analysis of seal performance for new type rotating ball valve with double direction metal sealing. *J. Cent. South Univ. Sci. Technol.* **2010**, *43*, 1345–1350.
19. Ahn, J.T.; Lee, K.C.; Lee, K.H.; Han, S.H. Investigation of the Mechanical Behavior of a Flexible Solid Metal Seal for a Cryogenic Butterfly Valve. *J. Mech. Sci. Technol.* **2011**, *25*, 2393–2400. [CrossRef]
20. Feyzullahoğlu, E. Abrasive wear, Thermal and viscoelastic behaviors of rubber seal materials used in different working conditions. *Proc. Inst. Mech. Eng. Part J J. Eng. Tribol.* **2015**, *229*, 64–73. [CrossRef]
21. Phull, H.S. New developments in triple-offset butterfly valves. *World Pumps* **2004**, *456*, 40–44. [CrossRef]
22. Burdick, M.D.; Zweig, B.; Moreland, R.E. Linear Thermal Expansion of Artificial Graphites to 1370° C. *J. Res. Natl. Bur. Stand.* **1951**, *47*, 35–40. [CrossRef]
23. ASME. ASME. ASME Boiler and Pressure Vessel Code, Section II—Materials. In *ASME Boiler and Pressure Vessel Code*; ASME: New York, NY, USA, 2013.
24. American Water Works Association. *American Water Works Association (AWWA) Manual M49, Butterfly Valves: Torque, Head Loss, and Cavitation Analysis*, 2nd ed.; American Water Works Association: Mumbai, India, 2012.
25. Kwak, H.; Seong, H.; Kim, C. Design of laminated seal in cryogenic triple-offset butterfly valve used in LNG marine engine. *Int. J. Precis. Eng. Manuf.* **2019**, *20*, 243–253. [CrossRef]
26. ASME. *B.16.34 Valves-Flanged, Threaded, and Welding End*; ASME: New York, NY, USA, 2014.